



Spectral shaping of lasing in vertically aligned coupled nanowire lasers

RAN DITCOVSKI^{1,*} AND TAL ELLENBOGEN^{1,2}

¹*Department of Physical Electronics, School of Electrical Engineering, Tel-Aviv University, Tel Aviv, 6997801, Israel*

²*Center for Light-Matter Interaction, Tel-Aviv University, Tel-Aviv 6779801, Israel*

*ditkovsk@post.tau.ac.il

Abstract: We use numerical simulations to study the effects of nanowire geometry on the emission spectra of nanowire-based lasers. The studied nanowire lasers are made from gallium-nitride and the simulations are performed using finite difference time domain method. We show that changes in the diameter of the nanowire lasers also change the effective refractive index of their optical guided modes, which allows control over their Fabry–Perot spectrum. In addition, we show that evanescent coupling of two vertically standing nanowire lasers, having different cross section sizes, leads to a Vernier effect, which results in single mode emission from the small footprint coupled lasers system.

© 2017 Optical Society of America

OCIS codes: (140.3325) Laser coupling; (140.5960) Semiconductor lasers; (310.6628) Subwavelength structures, nanostructures; (350.4238) Nanophotonics and photonic crystals.

References and links

1. P. Yang, R. Yan, and M. Fardy, “Semiconductor nanowire: what’s next?” *Nano Lett.* **10**(5), 1529–1536 (2010).
2. R. Yan, D. Gargas, and P. Yang, “Nanowire photonics,” *Nat. Photonics* **3**(10), 569–576 (2009).
3. M. Zimmler, J. Bao, F. Capasso, S. Müller, and C. Ronning, “Laser action in nanowires: observation of the transition from amplified spontaneous emission to laser oscillation,” *Appl. Phys. Lett.* **93**(5), 051101 (2008).
4. C. Z. Ning, “Semiconductor nanowire lasers,” *Semicond. Semimet.* **86**, 455–486 (2012).
5. M. H. Huang, S. Mao, H. Feick, H. Yan, Y. Wu, H. Kind, E. Weber, R. Russo, and P. Yang, “Room-temperature ultraviolet nanowire nanolasers,” *Science* **292**(5523), 1897–1899 (2001).
6. Y. Ma, X. Guo, X. Wu, L. Dai, and L. Tong, “Semiconductor nanowire lasers,” *Adv. Opt. Photonics* **5**(3), 216–273 (2013).
7. C. Couteau, A. Larrue, C. Wilhelm, and C. Soci, “Nanowire lasers,” *Nanophotonics* **4**(1), 90–107 (2015).
8. Q. Li, J. B. Wright, W. W. Chow, T. S. Luk, I. Brener, L. F. Lester, and G. T. Wang, “Single-mode GaN nanowire lasers,” *Opt. Express* **20**(16), 17873–17879 (2012).
9. X. Duan, Y. Huang, R. Agarwal, C. M. C. M. Lieber, and C. G. Fast, “Single-nanowire electrically driven lasers,” *Nature* **421**(6920), 241–245 (2003).
10. D. Saxena, S. Mokkapatil, P. Parkinson, N. Jiang, Q. Gao, H. H. Tan, and C. Jagadish, “Optically pumped room-temperature GaAs nanowire lasers,” *Nat. Photonics* **7**(12), 963–968 (2013).
11. B. Mayer, D. Rudolph, J. Schnell, S. Morkötter, J. Winnerl, J. Treu, K. Müller, G. Bracher, G. Abstreiter, G. Koblmüller, and J. J. Finley, “Lasing from individual GaAs-AlGaAs core-shell nanowires up to room temperature,” *Nat. Commun.* **4**, 2931–2939 (2013).
12. A. Hurtado, D. Jevtics, B. Guilhabert, Q. Gao, H. H. Tan, C. Jagadish, and M. D. Dawson, “Novel nanoscale transfer printing technique for precise positioning of nanowire lasers,” *SPIE Newsroom* (2017).
13. D. J. Gargas, M. E. Toimil-Molares, and P. Yang, “Imaging single ZnO vertical nanowire laser cavities using UV-laser scanning confocal microscopy,” *J. Am. Chem. Soc.* **131**(6), 2125–2127 (2009).
14. S. Chu, G. Wang, W. Zhou, Y. Lin, L. Chernyak, J. Zhao, J. Kong, L. Li, J. Ren, and J. Liu, “Electrically pumped waveguide lasing from ZnO nanowires,” *Nat. Nanotechnol.* **6**(8), 506–510 (2011).
15. R. Chen, T.-T. D. Tran, K. W. Ng, W. S. Ko, L. C. Chuang, F. G. Sedgwick, and C. Chang-Hasnain, “Nanolasers grown on silicon,” *Nat. Photonics* **5**(3), 1–18 (2011).
16. Y. Xiao, C. Meng, X. Wu, and L. Tong, “Single mode lasing in coupled nanowires,” *Appl. Phys. Lett.* **99**(2), 023109 (2011).
17. L. A. Coldren and S. W. Corzine, *Diode Lasers and Photonic Integrated Circuits* (John Wiley & Sons, 1997).
18. J. B. Wright, S. Campione, S. Liu, J. A. Martinez, H. Xu, T. S. Luk, Q. Li, G. T. Wang, B. S. Swartzentruber, L. F. Lester, and I. Brener, “Distributed feedback gallium nitride nanowire lasers,” *Appl. Phys. Lett.* **104**(4), 041107 (2014).
19. Y. Xiao, C. Meng, P. Wang, Y. Ye, H. Yu, S. Wang, F. Gu, L. Dai, and L. Tong, “Single-nanowire single-mode laser,” *Nano Lett.* **11**(3), 1122–1126 (2011).

20. H. Gao, A. Fu, S. C. Andrews, and P. Yang, "Cleaved-coupled nanowire lasers," *Proc. Natl. Acad. Sci. U.S.A.* **110**(3), 865–869 (2013).
21. H. Xu, J. B. Wright, T. Luk, J. J. Figiel, K. Cross, L. F. Lester, G. T. Wang, I. Brener, and Q. Li, "Single-mode lasing of GaN nanowire-pairs," *Appl. Phys. Lett.* **101**(11), 113106 (2012).
22. S. Adachi, "Optical constants of crystalline and amorphous semiconductors: numerical data and graphical information (Springer USA, 1999).
23. S. H. Chang and A. Taflove, "Finite-difference time-domain model of lasing action in a four-level two-electron atomic system," *Opt. Express* **12**(16), 3827–3833 (2004).
24. S. Gradečak, F. Qian, Y. Li, H.-G. Park, and C. M. Lieber, "GaN nanowire lasers with low lasing thresholds," *Appl. Phys. Lett.* **87**(17), 173111 (2005).
25. A. V. Maslov and C. Z. Ning, "Modal gain in a semiconductor nanowire laser with anisotropic bandstructure," *IEEE J. Quantum Electron.* **40**, 1389–1397 (2004).
26. H. Xu, J. B. Wright, A. Hurtado, Q. Li, T.-S. Luk, J. J. Figiel, K. Cross, G. Balakrishnan, L. F. Lester, I. Brener, and G. T. Wang, "Gold substrate-induced single-mode lasing of GaN nanowires," *Appl. Phys. Lett.* **101**(22), 221114 (2012).
27. B. E. A. Saleh, M. C. Teich, and B. E. Saleh, *Fundamentals of Photonics* (John Wiley & Sons, 1991).
28. K. Seo, M. Wober, P. Steinvurzel, E. Schonbrun, Y. Dan, T. Ellenbogen, and K. B. Crozier, "Multicolored vertical silicon nanowires," *Nano Lett.* **11**(4), 1851–1856 (2011).
29. B. M. Rey, R. Elnathan, R. Ditcovski, K. Geisel, M. Zanini, M.-A. Fernandez-Rodriguez, V. V. Naik, A. Frutiger, W. Richtering, T. Ellenbogen, N. H. Voelcker, and L. Isa, "Fully tunable silicon nanowire arrays fabricated by soft nanoparticle templating," *Nano Lett.* **16**(1), 157–163 (2016).
30. A. V. Maslov and C. Z. Ning, "Reflection of guided modes in a semiconductor nanowire laser," *Appl. Phys. Lett.* **83**(6), 1237–1239 (2003).
31. S. Xu, Y. Wei, M. Kirkham, J. Liu, W. Mai, D. Davidovic, R. L. Snyder, and Z. L. Wang, "Patterned growth of vertically aligned ZnO nanowire arrays on inorganic substrates at low temperature without catalyst," *J. Am. Chem. Soc.* **130**(45), 14958–14959 (2008).

1. Introduction

Semiconducting nanowires (NWs) show promising results in many potential applications including solar cells, bio-sensors, and thermoelectric devices [1,2]. The small dimensions of nanowires and the high refractive index of many semiconductors near their bandgap, lead to strong confinement of photons in the transverse dimension and guiding of photons in the longitudinal dimension. These features make such NWs interesting one dimensional photonic systems. Furthermore, a large impedance mismatch at the nanowire facets leads to formation of natural optical cavities. Together with the ability of NWs to provide optical gain, these features can be used to fabricate ultra-compact lasers [3]. This makes NWs attractive as integrated compact coherent light sources [2,4].

Since the first demonstration of amplified spontaneous emission in zinc oxide NWs by Huang et al. in 2001 [5], many groups have studied lasing action in NWs based on different materials [6,7]. Most studies to date have involved either a single NW lying on a substrate [3,8–12] or randomly grown, vertically standing, NWs [13–15]. Neither of these configurations is ideal for investigating the dynamics and interactions of large scale arrays of NW lasers, nor for developing nanowire based laser networks. Another disadvantage of nanowire lasers is that they emit light at multiple frequencies similar to a simple Fabry–Perot cavity [16]. For many applications, such as optical communications on a single chip, and spectroscopic detection, monochromaticity is of great importance. Therefore, there is a need to develop single mode NW lasers. One solution to this problem is to shorten the NW laser cavity until it will support only one longitudinal mode. However, shortening the laser also reduces the volume of gain material and increases the mirror loss from the end facets of the laser, to a degree where the lasing threshold might become prohibitively high. Another solution is to use the distributed feedback (DFB) technique which was proven to be very successful in semiconductor and fiber lasers. This technique involves fabricating a spectral filter by periodic modulation of the refractive index to satisfy the Bragg condition [17]. Achieving it in vertically standing NWs involves complicated fabrication processes. However, using a grating as the substrate of lying NW was proven to generate single mode lasing successfully [18].

A more viable solution, which has been demonstrated on NWs lying randomly on substrates, is to leverage the Vernier effect [16,19–21] to achieve single mode lasing from coupled NW cavities. Here we study a new configuration of vertically standing NW lasers and show that by manipulating their diameter we can tune the wavelengths of their oscillating longitudinal modes. By further controlling the geometrical parameters and spatial arrangement of two evanescently coupled standing NW lasers of the same length, the spectral emission from the NW lasers can be shaped to enable single mode lasing. Moreover, its miniature size and monochromaticity make this configuration suitable for applications such as optical communications on chip and spectroscopic detection. In addition, this configuration is highly scalable, making it suitable for studying the coupling dynamics of very large networks of NW lasers.

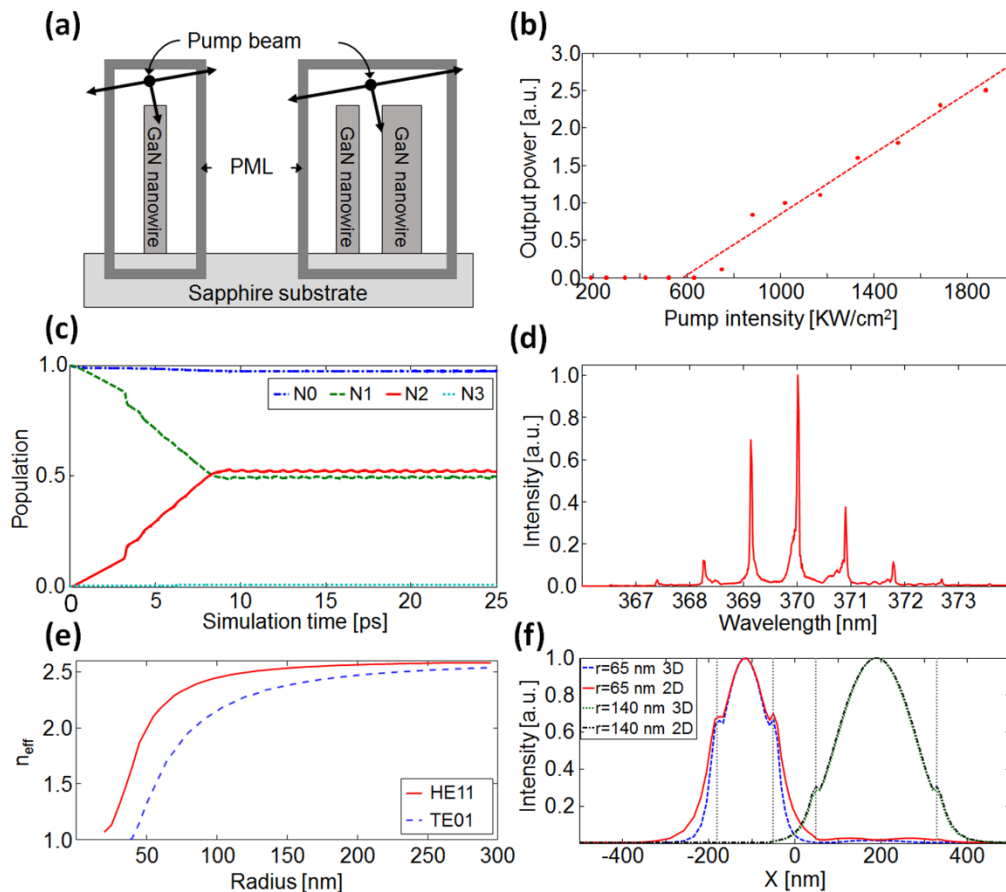


Fig. 1. Lasing simulations of nanowire lasers. (a) Simulation setup of single NW laser (left) and coupled cavity NWs laser (right); (b) Simulated light-in light-out curve of a single GaN NW; (c) Electron population of the four lasing levels as simulated by the FDTD's auxiliary differential equation (ADE). At $t \approx 8$ population inversion between the levels N_1 and N_2 is achieved and maintained until the end of the simulation; (d) Simulated lasing spectra of single GaN NW standing on sapphire substrate; (e) Change of the effective refractive index as a function of NW radius for the two lowest guided modes; (f) Comparison of the lowest guided modes (HE11) of a coupled cavity in 2D and 3D simulations.

2. Nanowire lasers simulations

The configurations that we study are based on single or dimer NW lasers as shown in Fig. 1(a). The NWs are made from GaN, which has been used in numerous NW laser studies. The

optical properties of GaN are well known [22] and can be simulated with great confidence. For the optical simulations we used commercial finite-difference time-domain (FDTD) software (Lumerical's FDTD) and modeled the material gain using the 4 levels 2 electron auxiliary differential equation (ADE) method developed by Chang et al. [23]. The suitability of describing the gain in NW lasers as a four level system was discussed elsewhere [7] and found adequate for NW with diameter larger than several tens of nanometers. In addition, this method takes into account effects of spontaneous emission and pump blocking due to Pauli exclusion principle. The parameters that we used for modeling the gain of GaN are shown in Table 1. The angular frequency and damping coefficients are discussed later in the text and the four decay lifetime parameters are typical values of semiconductor lasers [17].

The NWs in the simulations are optically pumped by a plane wave of wavelength, $\lambda_p = 267 \text{ nm}$ ($\omega = 7.05 \times 10^{15} \text{ rad/s}$), which coincides with the fourth harmonic of an Nd:YAG laser commonly used to pump GaN NW lasers [8,20,24]. The pump beam is injected from the top of the simulation area at a tilt of 10 degrees [Fig. 1(a)] as was previously done experimentally [5]. The pump coupling efficiency is in the range of 5% to 10%, depending on NW radius. The entire simulation region is meshed with a $\lambda_{em} / 20n \approx 7 \text{ nm}$ grid, where $\lambda_{em} \approx 370 \text{ nm}$ ($\omega = 5.09 \times 10^{15} \text{ rad/s}$) is the emission wavelength, and $n \approx 2.66$ is the refractive index close to the bandgap of GaN. The simulation area is enclosed by a perfectly matching layer (PML), which absorbs electromagnetic wave that propagates outward. During the simulation, all six components of the electromagnetic field are recorded inside and above the nanowires.

Table 1. Parameters for simulating GaN lasing by the 4-level 2-electron model.

| Parameter | Symbol | Value | Unit |
|--|------------|---------|-------|
| Angular frequency of the energy difference of levels 2-1 | ω_a | 5.09e15 | rad/s |
| Angular frequency of the energy difference of levels 3-0 | ω_b | 7.05e15 | rad/s |
| Damping coefficient, levels 2-1 | γ_a | 6.1e13 | rad/s |
| Damping coefficient, levels 3-0 | γ_b | 6.1e13 | rad/s |
| Decay lifetime from level 3 to 0 | t_{30} | 1e-9 | s |
| Decay lifetime from level 3 to 2 | t_{32} | 1e-13 | s |
| Decay lifetime from level 2 to 1 | t_{21} | 1e-9 | s |
| Decay lifetime from level 1 to 0 | t_{10} | 1e-13 | s |

To reduce the computational complexity of the FDTD simulations of isolated nanowires, we took into account the azimuthal symmetry of the nanowire and performed 2D simulations. This 2D reduction has already been used for simulating the reflections and confinement factor of guided modes and for calculating the modal gain in nanowires [25]. To test the simulation setup, we investigated the pump intensity-dependent emission from a single vertical GaN NW with radius, $r = 65 \text{ nm}$, and length, $L = 10 \mu\text{m}$. The NW was placed on top of a sapphire wafer, which is a common substrate for growing GaN nanowires [8,24]. Figure 1(b), shows the light-in light-out curve of the simulated NW laser. A typical laser curve was observed with a lasing threshold at $P_{th} = 590 \text{ KW/cm}^2$ and a linear increase of output power after the threshold. The lasing threshold intensity was nearly constant for NWs' radii in the range

between 60–300 nm. The value of the simulated threshold was of the same order of magnitude as those of previous experimental threshold measurements [8,26].

The time dependent populations of the four lasing energy levels, when pumped above the threshold at a power of 880KW/cm², are plotted in Fig. 1(c), where N_{0-3} are the conventional levels of a four level laser system [27]. At $t \approx 8$ ps, population inversion of levels N_1 and N_2 occurs and remains steady until the end of the simulation time. The emitted spectrum above the lasing threshold of the NW laser is shown in Fig. 1(d). Longitudinal Fabry–Perot modes are clearly shown, with a full width at half maximum (FWHM) of ~ 0.1 nm, and mode spacing of ~ 1.0 nm. The distance between these peaks, also called the free spectral range (FSR), is given by [20]:

$$\Delta\lambda = \frac{1}{L} \left(\frac{\lambda^2}{2n_g} \right) \quad (1a)$$

$$n_g = n_{\text{eff}} - \lambda \frac{dn_{\text{eff}}}{d\lambda} \quad (1b)$$

where $\Delta\lambda$ is the FSR, L is the NW length, λ is the wavelength in air, n_g is the group index and n_{eff} is the effective refractive index of the guided mode. The simulated mode spacing observed in Fig. 1(d) fits the expected theoretical mode spacing, predicted by Eq. (1), for NWs of these dimensions, with bulk refractive index $n = 2.66$ and chromatic dispersion $dn/d\lambda \approx -0.009 \text{ nm}^{-1}$ [22].

Changing the radius of the nanowires allows control over the effective refractive index of the modes [28,29] and can therefore be used to control the lasing characteristics. In Fig. 1(e) the change of n_{eff} as a function of the NW radius is shown for the transverse modes HE₁₁ and TE₀₁, which have the lowest lasing gain threshold and are the most probable modes to lase [25,30]. When combined with Eq. (1) this relation connects the FSR and the radius of the NW, which means that changing the radius of the NW lasers also changes the wavelengths of the oscillating Fabry–Perot modes.

We used the connection between the FSR and the NW radius to design a coupled cavity of two vertical NW lasers that share only one longitudinal mode and therefore emit single-mode coherent light. The first step in the design process is to find the guided modes of NW lasers, having various radii, and select two NWs with different radii that share one longitudinal mode. Then, the length of the NWs is calculated to determine the wavelength of the mutual longitudinal mode. Finally, the separation between the NWs is optimized to determine efficient coupling of the modes.

In the case of isolated single NWs, optical modes can be found using 2D simulations with great confidence. However, because the azimuthal symmetry brakes in the case of a coupled cavity of two nanowire lasers, we checked the validity of our 2D simulations by comparison with full 3D simulations. In Fig. 1(f) we show that the guided mode shapes of the 2D and 3D coupled cavity are similar. However, the small differences between 2D and 3D modes, especially at the coupled region, must be taken into account when determining the separation between two coupled cavity nanowires. In 2D simulations the coupled part of the optical mode was slightly larger than in the 3D case. As a result the optimized separation between the NWs in the 2D simulation was slightly larger than in the full 3D case.

3. Coupled cavity NW lasers

The underlying idea behind the single mode lasing is based on the Vernier effect as presented in Fig. 2. The longitudinal mode cavity function of NWs is given by their Fabry-Perot spectral response:

$$I = I_0 / \left[(1-r)^2 + 4r \sin^2 \left(n_g \pi L / \lambda_0 \right) \right] \quad (2)$$

where I is the intensity in the cavity, I_0 is the intensity of the initial wave, r is the reflection from the resonator facets, n_g is the diameter dependent group index, L is the length of the NW and λ_0 is the free space wavelength. It is clear that the modes of the coupled cavity, formed out of cavity a and cavity b , will satisfy the condition: $\Delta\lambda_{a+b} = M\Delta\lambda_a = N\Delta\lambda_b$, where M and N are integers. This condition, together with Eq. (1), gives us the ratio of the effective indices of the single NW lasers, $n_g^a / n_g^b = N / M$. However since in our simulation $dn_{\text{eff}} / d\lambda$ is very small, $\sim 0.001 \text{nm}^{-1}$, we can neglect the second term in Eq. (1b) and get $n_{\text{eff}}^a / n_{\text{eff}}^b = N / M$. To make sure that the coupled cavity has only one mode over the gain window, we can select N to be the number of modes that are supported by the thinner NW. This is because the thicker NW will have a smaller FSR, and thus, it can support more modes over the gain window than the thinner NW. We limit our design to a thicker NW that supports only one additional longitudinal mode, $M = N + 1$, in order to avoid non-physical values of the effective index. From simulation results we found that a NW laser of length $L = 10 \mu\text{m}$, and radius $r_a = 65 \text{nm}$, supported 7 longitudinal modes over the entire gain window and its transversal mode's effective index is $n_{\text{eff}}^a = 2.22$ [Fig. 1(e)]. Using the ratio of the effective indices we calculated the required effective index of the thicker laser to be $n_{\text{eff}}^b = 2.53$, which fits to a NW having a radius of $r_b = 140 \text{nm}$. We are using the effective index curve for the HE11 mode, even though for NW radius above 90 nm the TE01 mode will have the lowest gain threshold. This is because the coupled lasers simulations show that on both NWs the mode that lase is HE11. In Fig. 2 we can see that for two lasers with these radii there is only one mutual longitudinal mode within the gain bandwidth, which is given by the damping coefficient, γ_a (Table 1). We used a fixed value of $\gamma_a = 61 \text{THz}$, which corresponds to photoluminescence spectral bandwidth that was measured in previous experiments on GaN nanowires lasers [8], [21]. The wavelength of this mode can be controlled by changing the length of the coupled lasers.

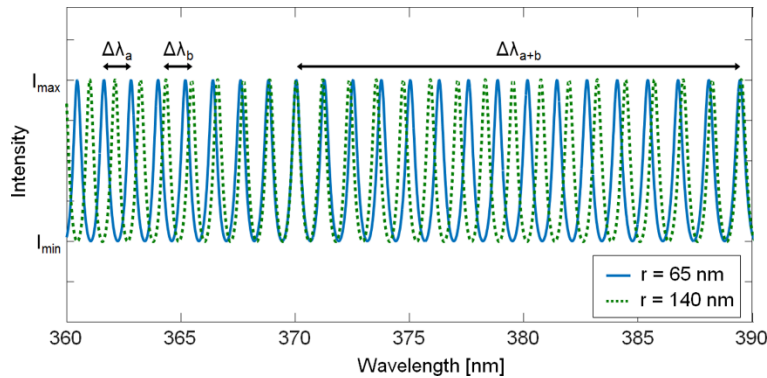


Fig. 2. Calculated cavity function for NWs with $r_a = 65 \text{nm}$ and $r_b = 140 \text{nm}$.

The allowed longitudinal modes are those where the cavity length is a multiple of half the mode's effective wavelength. Thus, for a longitudinal mode of the coupled cavity this condition must hold separately for both NW cavities: $L = p(\lambda_0 / 2n_{\text{eff}}^a) = q(\lambda_0 / 2n_{\text{eff}}^b)$, where L is the cavity length, λ_0 is the mode's wavelength in air, $n_{\text{eff}}^{a,b}$ are the single NW cavity effective refractive indices of the guided mode, and p, q are integers. To find a cavity

length that satisfies these conditions, we can substitute, $p = q - m$, where m is also an integer, and find L . The expression for the cavity length is then, $L_m = \frac{1}{2} \lambda_0 m / \Delta n_{\text{eff}}$, where $\Delta n_{\text{eff}} = n_{\text{eff}}^b - n_{\text{eff}}^a$. This means that for any multiple of $L_1 = \frac{1}{2} \lambda_0 / \Delta n_{\text{eff}}$, the coupled cavity will support a longitudinal mode with wavelength λ_0 . For $\lambda_0 = 370$ nm and the effective indices that are presented above, $L_1 = 597$ nm. To keep the length as close as possible to the length of the single laser cavity we simulated above, we simulate the case of 17 times the minimal length $L \approx 10.1 \mu\text{m}$.

The last free parameter of the coupled cavity is the distance between the nanowires. To achieve significant coupling, the nanowires need to be as close as possible. However, if the coupling is too strong, it will modify the effective refractive index, the FSR and the wavelength of the longitudinal modes. To find the optimal distance, the effective refractive indexes of the lowest modes of each of the coupled cavity nanowires were calculated as a function of the NW separation [Fig. 3(a)]. Providing that the NW separation is greater than $D = 50$ nm the change in the effective refractive index is negligible. If we place the NWs in separation of less than $D = 50$ nm, even though the coupling will increase, the effective refractive index of the NW modes might change in a way that allows more than one mutual longitudinal mode. On the other side, if the separation will be too large, the coupling between the NWs will weaken to a degree where different longitudinal modes might lase in each NW. In Fig. 3(b) the shape of the lowest mode of each NW is shown at a separation of $D = 100$ nm. At this distance the change of the effective refractive index is small, and the FSR change is less than 1%.

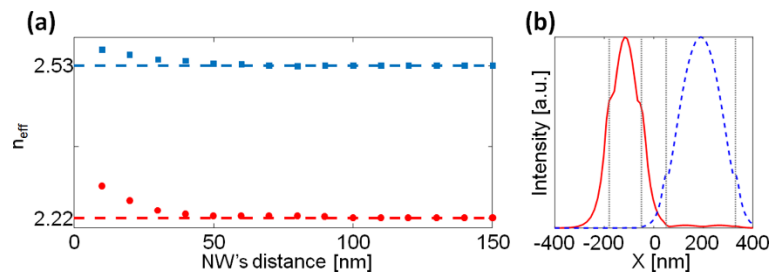


Fig. 3. Coupling of coupled cavity modes (2D simulation). (a) Effective refractive index of the two lowest modes of a coupled cavity increase with decreasing separation between the NWs. Dashed line represents the value of n_{eff} of each single NW lowest mode; (b) The lowest modes, HE₁₁, of the single NWs that form the coupled cavity ($r_a = 65$ nm ; $r_b = 140$ nm ; $D = 100$ nm). The change of n_{eff} caused an FSR change of less than 1%.

The coupled cavity lasing simulations for these parameters are shown in Fig. 4(a). The lasing threshold of the coupled cavity is $990 \text{KW} / \text{cm}^2$, which is $\sim 67\%$ higher than that of the single NW laser of $10 \mu\text{m}$ length. On the middle and bottom graphs of Fig. 4(a) we can see multimode spectra of the single NW lasers that made this cavity. On the upper graph, the spectrum of the coupled cavity laser exhibit only one longitudinal mode. This is the only lasing mode of the coupled cavity. We can see that there is a shift in the wavelength of the single mutual longitudinal mode in Fig. 4(a). The shift of the mutual mode has been shown experimentally in other works [16,19,20]. Here the redshift can be caused due to effective index changes caused by proximity of the NWs. In our simulations, we observed that the radius tolerance of each of the NWs for single mode lasing is in the range of 5-10 nm. Figure 4(b) shows the results of a simulation of a coupled cavity laser with nanowire radii

$r_a = 65$ nm (middle) and $r_b = 100$ nm (bottom). These radii do not meet the criteria for a single mutual longitudinal mode that we showed above and the simulation shows multimode lasing (top).

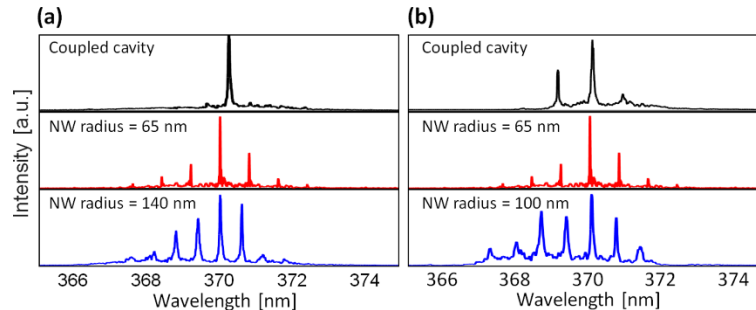


Fig. 4. Lasing simulation of coupled cavity NW laser (NWs separation is, $D = 100$ nm). (a) Lasing from a well-designed coupled cavity NW laser exhibits a single mode spectrum with side mode suppression of 12 dB (top). When separated, each NW exhibit multimode spectrum (middle: $r_a = 65$ nm and bottom: $r_b = 140$ nm); (b) Lasing spectrum of a poorly designed coupled cavity shows multiple longitudinal modes with side mode suppression of 2 dB (top). This coupled cavity is made from NWs with radii: $r_a = 65$ nm (middle) and $r_b = 100$ nm (bottom).

In Fig. 5, the dependence of the spectrum on NWs separation and radii tolerance are shown. As discussed earlier we see in Fig. 5(a) that when the separation is, $D = 20$ nm, the effective index of the modes changes, and the coupled cavity can support two mutual longitudinal modes. When the distance between the NWs is, $D = 250$ nm, the coupling weakens and other longitudinal modes begin to appear in the spectrum. The tolerance of the NWs radii is shown in Fig. 5(b). We see that in the case of a radius change of up to 10 nm in the thicker NW and 5 nm in the thinner NW, the lasing spectrum is still acceptably single mode. The reason of the tighter tolerance in the thinner NW is that the effective index changes more rapidly as the radius get small (Fig. 1(e)).

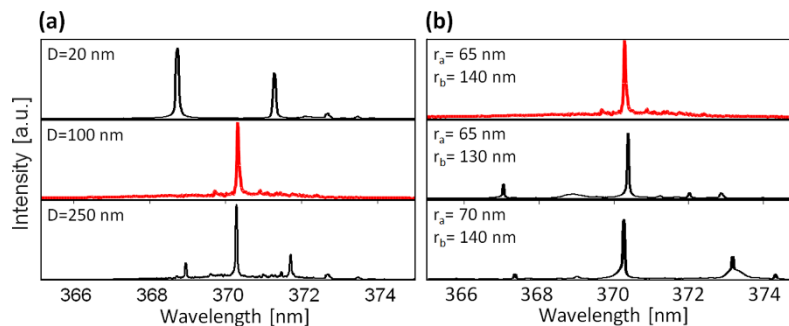


Fig. 5. (a) The effect of NW separation on the coupled cavity spectrum. Top: in a very close distance, $D = 20$ nm, two longitudinal modes lase in the mutual cavity. Middle: a single mode spectrum is shown for intermediate distance of, $D = 100$ nm. Bottom: when the separation is large, the coupling weakens and several longitudinal modes begin to appear in the spectrum; (b) Top: the single mode spectrum of a well design couple cavity. Middle: a 10 nm change in the thicker NW's radius still shows an acceptable single mode spectrum. Bottom: a 5 nm change in the thinner NW's radius shows a sharp mode in the middle of the spectrum with a side mode which is not fully suppressed. The tolerance of the thinner NW's radius is more sensitive than that of the thicker NW since the effective index changes faster as the radius is smaller.

4. Conclusions

To conclude, we simulated the lasing spectrum of vertically aligned GaN NW lasers using ADE-FDTD methods. We used this simulation tool to investigate the effects of the NW physical dimensions on the NW lasing spectrum. We demonstrated the effects of changing the length and radius of NW lasers on the wavelength of their longitudinal modes, thus, allowing control over the shape of the emission spectrum. In addition, we studied the configuration of a coupled cavity of two standing NWs. We showed that the configuration can be modified to lase in a single longitudinal mode based on the Vernier effect without shortening the cavity to be half effective wavelength. This studied configuration is highly scalable, using fabrication methods for growing large scale vertically standing ordered NW arrays [29,31], making it suitable for the design of large networks of nanowire lasers side by side.

Funding

This work was partially supported by the Israel Science Foundation grant no. 133113.